

# Warpage Prediction of Optical Media

BINGFENG FAN,<sup>1</sup> DAVID O. KAZMER,<sup>2</sup> WIT C. BUSHKO,<sup>3</sup> RICHARD P. THERIAULT,<sup>4</sup> ANDREW J. POSLINSKI<sup>4</sup>

<sup>1</sup>Department of Mechanical & Industrial Engineering, University of Massachusetts Amherst, Amherst, Massachusetts 01003

<sup>2</sup>Department of Plastics Engineering, University of Massachusetts Lowell, Lowell, Massachusetts 01854

<sup>3</sup>GE Corporate Research and Development, Schenectady, New York 12301

<sup>4</sup>GE Plastics, One Plastics Avenue, Pittsfield, Massachusetts 01201

*Received 5 September 2002; revised 18 December 2002; accepted 6 January 2003*

**ABSTRACT:** The warpage of injection–compression-molded optical media, such as compact discs and digital video discs, due to asymmetric cooling during production is predicted. Thermally induced stress is calculated with a nonisothermal compressible flow simulation with a viscoelastic constitutive model. A finite element analysis is formulated with axisymmetric plate elements based on Kirchhoff thin-plate theory to simulate the warpage of the disc due to the asymmetric thermal stress and gravity after demolding. Simulation results of warpage for compact-disc-recordable moldings are compared with experimental observations under different processing conditions, such as the melt temperature, mold temperature, and packing pressure, with an optical grade of polycarbonate. The comparison shows that the simulation well predicts the effects of various processing conditions. Both the simulation and experiment indicate that of the processing conditions, the mold temperature has the greatest effect on warpage. © 2003 Wiley Periodicals, Inc. *J Polym Sci Part B: Polym Phys* 41: 859–872, 2003

**Keywords:** warpage; optical media; polycarbonates; injection compression; residual stress; viscoelastic properties; compact disc molding; injection molding

## INTRODUCTION

Optical media such as compact discs (CDs) and digital video discs (DVDs) are typically injection–compression-molded with an optical grade of polycarbonate (PC). One critical quality of such mass-produced optical media is warpage caused by internal residual stresses, which reduces the dimensional stability of the discs and is particularly detrimental for DVDs because it hinders the bonding of multiple substrates and induces addi-

tional in-plane birefringence. There are many causes of the warpage of injection/injection–compression-molded parts. Paro et al.<sup>1</sup> offered various reasons for warpage, such as uneven cooling, flow orientation effect, uneven packing, and gate effect, providing schematic illustrations. In this study, the warpage induced by asymmetric thermal stress due to differential mold temperatures is studied, and simulation results of compact-disc-recordable (CD-R) moldings are compared with experimental observations under different processing conditions.

For the injection-molded or injection–compression-molded parts, there are two principal sources of residual stresses:<sup>2</sup> flow-induced stress and thermally induced stress. The first is due to the

Correspondence to: D. O. Kazmer (E-mail: david\_kazmer@uml.edu)

*Journal of Polymer Science: Part B: Polymer Physics*, Vol. 41, 859–872 (2003)  
© 2003 Wiley Periodicals, Inc.

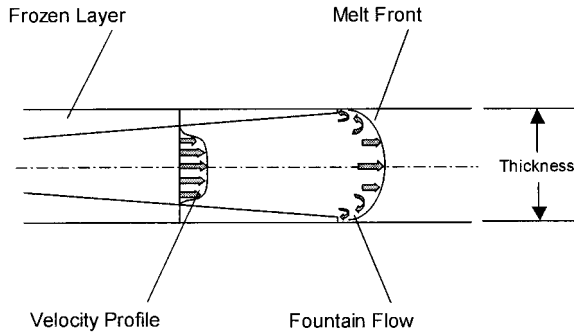


**Figure 1.** Schematic of polymer flow during mold filling.

shear flow during the filling and packing stages, and the shear and normal stresses developed are partly frozen-in due to the rapid cooling of the melt. The second type of residual stress arises during the cooling process of the injection-compression molding. As illustrated in Figure 1, when the hot polymer melt is injected into the relatively cold mold cavity under high pressure, a thin layer of the melt solidifies. As the part experiences further cooling, the solidification develops inward. Along the thickness direction of the part, the temperature distribution is highly nonuniform. Consequently, each material point through the thickness solidifies at a different time under a different pressure and experiences different shrinkage. The temperature and pressure history, coupled with the viscoelastic properties of the polymer during the rapid cooling process, results in the development of the thermally induced residual stresses. Although the flow-induced stresses are the main sources of molecular orientations and, therefore, the sources of anisotropic mechanical and optical properties between the flow and cross-flow directions, they are generally lower than the thermally induced stresses by one to two orders of magnitude. As such, the warpage of the disc is mainly caused by the thermally induced stresses.

Ideally, if the temperatures of the mold walls of the stationary and moving mold halves are exactly the same, the stress distribution across the thickness direction will be symmetrical with respect to the midplane of the disc; consequently, there will be no warpage in the molded disc. However, it is common to find a temperature difference between the two mold halves in practice because of the location of the gates, the difference in the coolant temperatures of both sides, or the stochastic deviation of the actual temperature

from the control parameters set on the machine. As a result, the gapwise distribution of the residual stress will no longer be symmetrical. Before ejection of the disc, the out-of-plane deformation is constrained by the mold walls. After ejection, the disc experiences free quench in the air and is free to deform. Because of the asymmetry of the internal stress, the disc will tend to warp to achieve a lower energy state.

## STRESS CONSTITUTIVE MODELS

The thermal stress calculation follows the methodology originated by Baaijens<sup>3</sup> with a linear viscoelastic constitutive model:

$$\boldsymbol{\sigma} = -p^h \mathbf{I} + \boldsymbol{\sigma}^d \quad (1)$$

$$p^h = -\frac{1}{3} \text{tr}(\boldsymbol{\sigma}) = \int_0^t \left( \frac{\alpha}{\kappa} \dot{T} - \frac{1}{\kappa} \text{tr}(\dot{\boldsymbol{\epsilon}}) \right) d\tau \quad (2)$$

$$\boldsymbol{\sigma}^d = \sum_{i=1}^m 2 \int_0^t g_i e^{-[\xi(t)-\xi(\tau)]/\theta_i} \dot{\boldsymbol{\epsilon}}^d d\tau \quad (3)$$

where  $\boldsymbol{\sigma}^d$  and  $\dot{\boldsymbol{\epsilon}}^d$  are the deviatoric stress and strain rate tensors, respectively;  $g_i$  and  $\theta_i$  are the shear moduli and the corresponding relaxation times for  $m$  number of modes, respectively;  $T$  is the temperature;  $p^h$  is the hydrostatic pressure; and  $\mathbf{I}$  is the unit tensor. The volume expansion coefficient,  $\alpha$ , and the isothermal compressibility coefficient,  $\kappa$ , are defined as follows:

$$\alpha = \frac{1}{\nu} \left( \frac{\partial \nu}{\partial T} \right)_P, \quad \kappa = -\frac{1}{\nu} \left( \frac{\partial \nu}{\partial P} \right)_T \quad (4)$$

which are obtained from the  $P$ - $\nu$ - $T$  relationship. The pseudotime  $\xi$  is defined as follows:

$$\xi(\tau) = \int_0^t \frac{1}{a_T(T)} ds \quad (5)$$

where  $a_T$  is the shift factor of the time-temperature superposition principle.

**Table 1.** Material Coefficients of the Tait Equation for PC

Coefficient	Value	Unit
$b_{1,l}$	$8.69 \times 10^{-4}$	m <sup>3</sup> /kg
$b_{2,l}$	$6.05 \times 10^{-7}$	m <sup>3</sup> /kg °C
$b_{3,l}$	$1.42 \times 10^8$	Pa
$b_{4,l}$	$3.89 \times 10^{-3}$	°C <sup>-1</sup>
$b_{1,s}$	$8.68 \times 10^{-4}$	m <sup>3</sup> /kg
$b_{2,s}$	$2.19 \times 10^{-7}$	m <sup>3</sup> /kg °C
$b_{3,s}$	$2.27 \times 10^8$	Pa
$b_{4,s}$	$2.27 \times 10^{-3}$	°C <sup>-1</sup>
$b_5$	143.29	°C
$b_6$	$3.81 \times 10^{-7}$	°C Pa <sup>-1</sup>

## MATERIAL CHARACTERIZATION

The simulation of the injection–compression–molding process, which provides temperature and pressure fields, is an integral part of the warpage prediction and has previously been described.<sup>4</sup> Material properties specified in the simulation by  $P$ – $v$ – $T$ , rheological, thermal, and viscoelastic models were characterized, and a fitting routine was developed to extract the material coefficients from the test data.

The  $P$ – $v$ – $T$  relationship is modeled by the Tait equation:<sup>5</sup>

$$\nu(T, P) = \nu_0(T) \left( 1 - 0.0894 \ln \left( 1 + \frac{P}{B(T)} \right) \right) \quad (6)$$

where for  $T > T_t(P)$ ,

$$\nu_0 = b_{1,l} + b_{2,l}(T - b_5), \quad (7)$$

$$B(T) = b_{3,l} \exp(-b_{4,l}(T - b_5)) \quad (8)$$

and for  $T < T_t(P)$ ,

$$\nu_0 = b_{1,s} + b_{2,s}(T - b_5), \quad (9)$$

$$B(T) = b_{3,s} \exp(-b_{4,s}(T - b_5)) \quad (10)$$

$T_t(P) = b_5 + b_6 P$ ,  $b_{1,l}$ – $b_{4,l}$ ,  $b_{1,s}$ – $b_{4,s}$ ,  $b_5$ , and  $b_6$  are material coefficients.

The viscosity is modeled by the modified Cross-WLF model:<sup>6</sup>

$$\eta(\dot{\gamma}, T, P) = \frac{\eta_0(T, P)}{1 + \left( \frac{\eta_0 \dot{\gamma}}{\tau^*} \right)^{1-n}} \quad (11)$$

with

$$\eta_0(T, P) = D_1 \exp \left( - \frac{A_1(T - T_t)}{A_2 + (T - T_t)} \right) \quad T > T_t(P) \quad (12)$$

$$\eta_0(T, P) = \infty \quad T < T_t(P) \quad (13)$$

$$T_t(P) = D_2 + D_3 P, \quad A_2 = \tilde{A}_2 + D_3 P \quad (14)$$

where  $n$  denotes the power-law index,  $\tau^*$  is a critical stress level at which  $\eta$  is in transition between the Newtonian limits,  $\eta_0$  is the zero-shear-rate viscosity,  $\dot{\gamma}$  is the shear rate, and  $T_t$  is a transition temperature. The parameters ( $n$ ,  $\tau^*$ ,  $D_1$ ,  $D_2$ ,  $D_3$ ,  $A_1$ , and  $\tilde{A}_2$ ) are material coefficients, which are determined by the fitting of shear-viscosity test data.

The following empirical functional forms from Chiang et al.<sup>7</sup> are used to model the variable specific heat and thermal conductivity of PC for the temperature field calculation:

$$C_p(T) = c_1 + c_2(T - C_5) + c_3 \tanh(c_4(T - C_5)) \quad (15)$$

$$k(T) = \lambda_1 + \lambda_2(T - \lambda_5) + \lambda_3 \tanh(\lambda_4(T - \lambda_5)) \quad (16)$$

where  $c_1$ – $c_5$  and  $\lambda_1$ – $\lambda_5$  are material-dependent coefficients.

The storage modulus  $G'$  and the loss modulus  $G''$  of PC are measured by dynamic mechanical test in the temperature range of 100–280 °C. The test data are shifted to a reference temperature of 150 °C to generate the master curves. The shear relaxation modulus is modeled by a set of discrete

**Table 2.** Material Coefficients of Viscosity for PC

Coefficient	Value	Unit
$n$	0.006	
$\tau^*$	$9.31 \times 10^5$	Pa
$D_1$	$7.33 \times 10^5$	Pa s
$D_2$	143.29	°C
$D_3$	0	°C Pa <sup>-1</sup>
$A_1$	17.19	
$\tilde{A}_2$	140.80	°C

**Table 3.** Material Coefficients of Specific Heat for PC

Coefficient	Value	Unit
$c_1$	$1.56 \times 10^3$	J/kg °C
$c_2$	3.02	J/kg °C <sup>2</sup>
$c_3$	$7.27 \times 10^1$	J/kg °C
$c_4$	$4.64 \times 10^{-1}$	°C <sup>-1</sup>
$c_5$	140.96	°C

moduli  $g_i$  and relaxation times  $\theta_i$ , determined by the fitting of the master curves of  $G'$  and  $G''$ . The time-temperature shift factor is fitted by the WLF equation<sup>8</sup> for temperatures above 150 °C

$$\log(a_T) = -\frac{C_1(T - T_{\text{ref}})}{C_2 + (T - T_{\text{ref}})} \quad (17)$$

and by the following equation for temperatures below 150 °C:

$$\log(a_T) = \frac{a(1 - e^{-(b(T_{\text{ref}} - T))^c})}{d + e^{-(b(T_{\text{ref}} - T))^c}} \quad (18)$$

where  $T_{\text{ref}}$  is the reference temperature and  $C_1$ ,  $C_2$ ,  $a$ ,  $b$ ,  $c$ , and  $d$  are material coefficients.

The material coefficients are provided in Table 1–6, with the material test data and fitted curves shown in Figure 2–7.

## FINITE ELEMENT FORMULATION

After the demolding, the warpage of the disc is modeled by a finite element analysis (FEA). The elements chosen are two-node, one-dimensional axisymmetric thin-plate elements discretized along the radial direction. Each node has three degrees of freedom

**Table 4.** Material Coefficients of Thermal Conductivity for PC

Coefficient	Value	Unit
$\lambda_1$	$2.58 \times 10^{-1}$	W/m °C
$\lambda_2$	$3.95 \times 10^{-4}$	W/m °C <sup>2</sup>
$\lambda_3$	$5.11 \times 10^{-2}$	W/m °C
$\lambda_4$	$-7.06 \times 10^{-1}$	°C <sup>-1</sup>
$\lambda_5$	175.70	°C

**Table 5.** Relaxation Moduli and Relaxation Times of PC

$g_i$ (Pa)	$\theta_i$ (s)
$1.11 \times 10^7$	$2.92 \times 10^{-10}$
$9.21 \times 10^6$	$3.60 \times 10^{-9}$
$1.39 \times 10^7$	$3.41 \times 10^{-8}$
$2.16 \times 10^7$	$2.80 \times 10^{-7}$
$5.55 \times 10^7$	$2.80 \times 10^{-6}$
$1.38 \times 10^8$	$3.12 \times 10^{-5}$
$3.28 \times 10^8$	$4.45 \times 10^{-4}$
$2.75 \times 10^8$	$4.50 \times 10^{-3}$
$3.30 \times 10^7$	$3.79 \times 10^{-2}$
$1.41 \times 10^6$	3.34
$7.93 \times 10^5$	$5.65 \times 10^1$
$4.55 \times 10^5$	$3.84 \times 10^2$
$2.36 \times 10^5$	$1.93 \times 10^3$
$4.03 \times 10^4$	$7.00 \times 10^3$
$7.59 \times 10^3$	$2.40 \times 10^4$

$$\mathbf{D} = [u \quad w \quad \varphi]^T$$

corresponding to radial and vertical displacement as well as rotation so that both in-plane and out-of-plane displacements can be considered.<sup>9</sup>

Each element along the radial direction,  $r$ , of the disc is divided into a number of layers along the thickness direction,  $z$ , to calculate the displacements and thermal stresses as a function of  $z$ . The thickness discretization is the same as in the calculation of the gapwise temperature distribution by the finite difference method. Because of the mold-filling process, the temperature distribution of the disc is not homogeneous along the radial direction. Therefore, the temperature and thermal stress are both functions of  $r$  and  $z$ .

## Main Assumptions of FEA

1. There is no transverse shear deformation. Therefore, normals to the midplane before

**Table 6.** Material Coefficients of the Time-Temperature Shift Factor for PC

Coefficient	Value	Unit
$T_{\text{ref}}$	150	°C
$C_1$	8.83	°C
$C_2$	35.70	°C
$a$	1.96	°C <sup>-1</sup>
$b$	0.13	°C <sup>-1</sup>
$c$	0.98	°C <sup>-1</sup>
$d$	0.25	°C <sup>-1</sup>

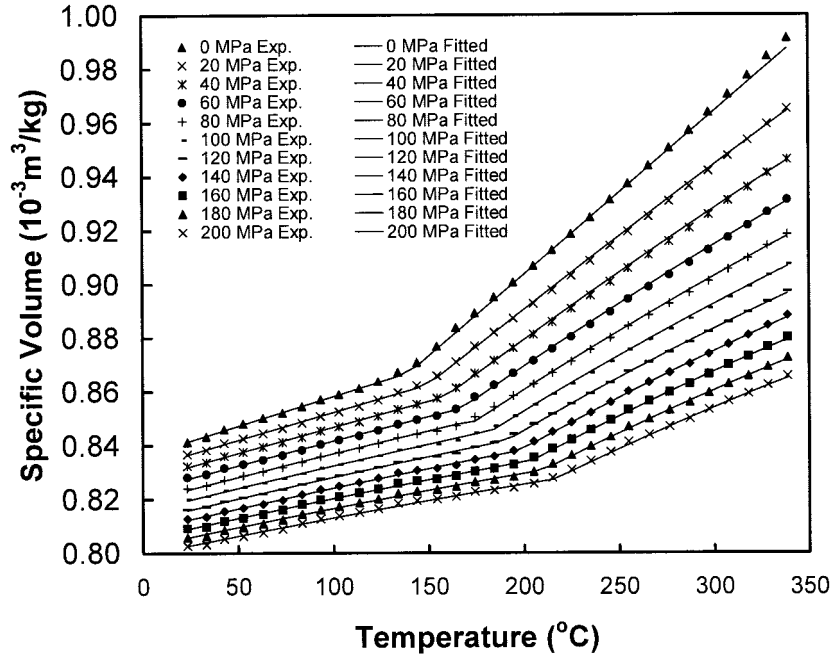


Figure 2. Specific volume of PC: experimental data and Tait equation fit.

deformation remain straight and normal to the midplane after deformation. This assumption is from the classical Kirchhoff thin-plate theory. Because the radius-to-thickness ratio of CDs and DVDs is generally greater than 50, the thin-plate assumption is justifiable.

2.  $u(r, z) = \bar{u}(r) - z\bar{\varphi}(r)$ , where  $\bar{\varphi}(r) =$

$d\bar{w}(r)/dr$  is the rotation and  $\bar{u}(r)$  and  $\bar{w}(r)$  are the radial and vertical displacements of the midplane of the disc. This assumption is relaxed compared with those in the literature<sup>9-12</sup> by the inclusion of the effect of radial displacement of the midplane on the radial displacement at different positions along the  $z$  direction.

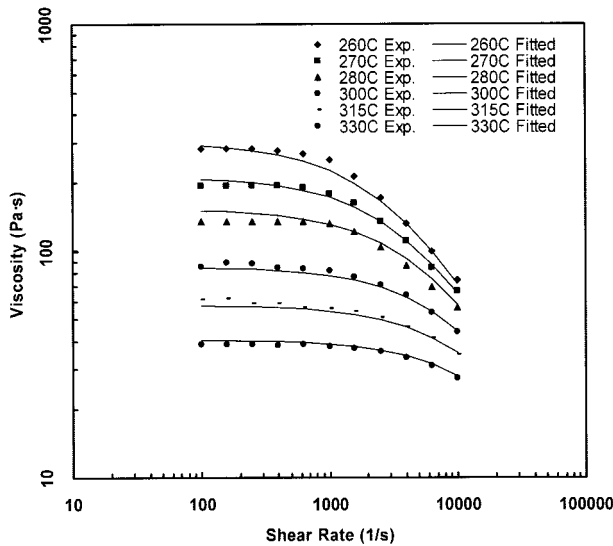


Figure 3. Viscosity of PC: experimental data and Cross-WLF model fit.

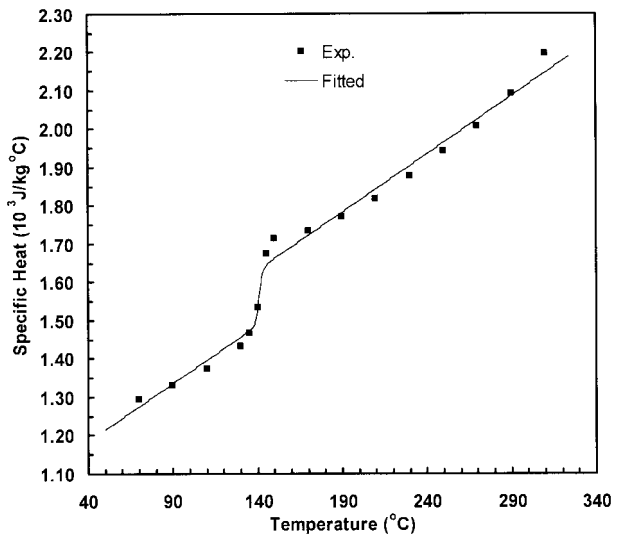
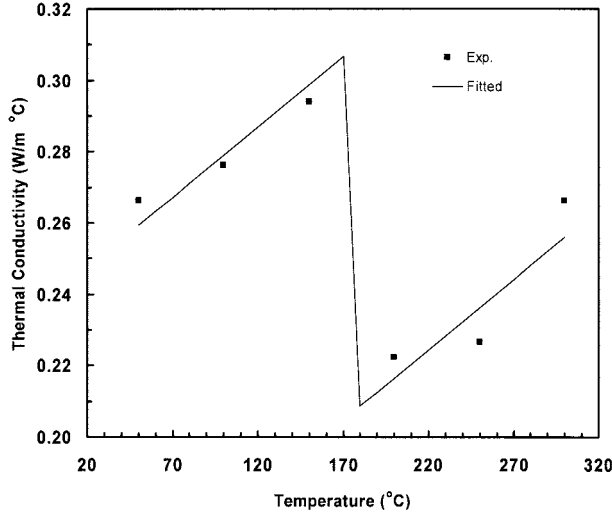


Figure 4. Specific heat of PC (refer to the text for the fitted model).



**Figure 5.** Thermal conductivity of PC (refer to the text for the fitted model).

3.  $w(r) = \bar{w}(r)$ , which means that the vertical displacement does not vary through the thickness.

**Strain–Displacement Relationships**

Because there are six degrees of freedom in each element, six coefficients have to be taken in the displacement interpolation polynomials. For the classical Kirchhoff thin-plate elements, the rotation is the derivative of the vertical displacement. Therefore, the vertical displacement interpolation function requires  $C^1$  continuity. Substituting the nodal displacement values of an element into trial displacement interpolation polynomials, we find that the unique solution requires the radial displacement to vary linearly in  $x$  and the vertical displacement to vary as a cubic in  $x$ , where  $x$  is the local coordinate of the radial direction. The displacement within an element can be described as follows:

$$\begin{Bmatrix} u \\ w \end{Bmatrix} = \begin{bmatrix} 1 - \xi & \frac{6z(\xi - \xi^2)}{s} & z(-1 + 4\xi - 3\xi^2) & \xi & \frac{6z(-\xi + \xi^2)}{s} & z(2\xi - 3\xi^2) \\ 0 & 1 - 3\xi^2 + 2\xi^3 & s(\xi - 2\xi^2 + \xi^3) & 0 & 3\xi^2 - 2\xi^3 & s(\xi^3 - \xi^2) \end{bmatrix} \begin{Bmatrix} \bar{u}_1 \\ \bar{w}_1 \\ \bar{\varphi}_1 \\ \bar{u}_2 \\ \bar{w}_2 \\ \bar{\varphi}_2 \end{Bmatrix} \quad (19)$$

where  $\xi$  is equal to  $x/s$ ,  $s$  is the length of the element, and  $[\bar{u}_1 \ \bar{w}_1 \ \bar{\varphi}_1 \ \bar{u}_2 \ \bar{w}_2 \ \bar{\varphi}_2]$  is the element nodal displacement vector of the midplane.

The strain–displacement relationships in cylindrical coordinate systems have the following form

$$\begin{Bmatrix} \varepsilon_{rr} \\ \varepsilon_{\theta\theta} \\ \kappa_{rr} \\ \kappa_{\theta\theta} \end{Bmatrix} = \begin{Bmatrix} \frac{du}{dr} \\ \frac{u}{r} \\ -\frac{d^2w}{dr^2} \\ -\frac{1}{r} \frac{dw}{dr} \end{Bmatrix} = \begin{Bmatrix} \frac{1}{s} \frac{du}{d\xi} \\ \frac{u}{r} \\ -\frac{1}{s^2} \frac{d^2w}{d\xi^2} \\ -\frac{1}{sr} \frac{dw}{d\xi} \end{Bmatrix} \quad (20)$$

With eq 19 substituted into eq 20, the strain–displacement relationships are derived:

$$\begin{Bmatrix} \varepsilon_{rr} \\ \varepsilon_{\theta\theta} \\ \kappa_{rr} \\ \kappa_{\theta\theta} \end{Bmatrix} = \begin{bmatrix} -\frac{1}{s} & \frac{6z}{s^2}(1 - 2\xi) & \frac{z}{s}(4 - 6\xi) & \frac{1}{s} & \frac{6z}{s^2}(-1 + 2\xi) & \frac{z}{s}(2 - 6\xi) \\ \frac{1 - \xi}{r} & \frac{6z}{rs}(\xi - \xi^2) & \frac{z}{r}(-1 + 4\xi - 3\xi^2) & \frac{\xi}{r} & \frac{6z}{rs}(-\xi + \xi^2) & \frac{z}{r}(2\xi - 3\xi^2) \\ 0 & \frac{6}{s^2}(1 - 2\xi) & \frac{2}{s}(2 - 3\xi) & 0 & \frac{6}{s^2}(2\xi - 1) & \frac{2}{s}(1 - 3\xi) \\ 0 & \frac{6}{sr}(\xi - \xi^2) & \frac{1}{r}(-1 + 4\xi - 3\xi^2) & 0 & \frac{6}{sr}(-\xi + \xi^2) & \frac{1}{r}(2\xi - 3\xi^2) \end{bmatrix} \begin{Bmatrix} \bar{u}_1 \\ \bar{w}_1 \\ \bar{\varphi}_1 \\ \bar{u}_2 \\ \bar{w}_2 \\ \bar{\varphi}_2 \end{Bmatrix} \quad (21)$$

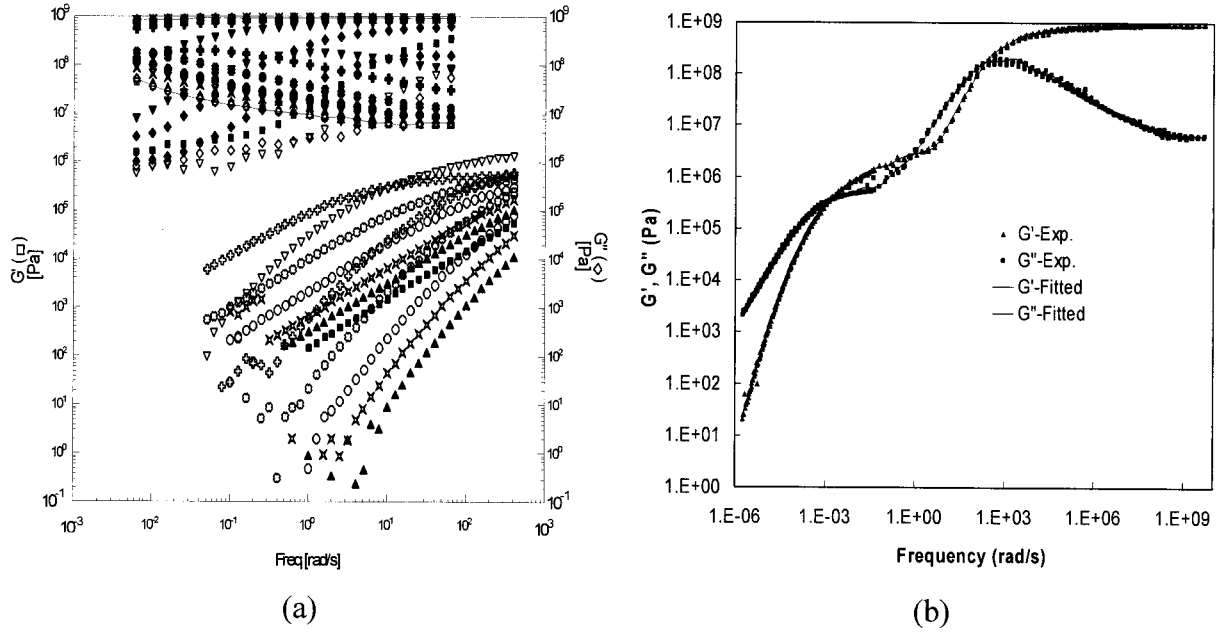


**Figure 6.** (a)  $G'$  and  $G''$  of PC measured at 100–280 °C and (b) corresponding master curves at a reference temperature of 150 °C.

where  $\varepsilon_{rr}$  and  $\varepsilon_{\theta\theta}$  are the radial and hoop strains, respectively, and  $\kappa_{rr}$  and  $\kappa_{\theta\theta}$  are the radial and

hoop curvatures, respectively. Equation 21 can be written as follows:

$$\boldsymbol{\varepsilon} = \sum_{i=1}^2 \mathbf{B}_i \bar{\mathbf{u}}_i \quad (22)$$

where  $\boldsymbol{\varepsilon}$  is the element strain vector,  $\mathbf{B}_i$  is the strain–displacement matrix, and  $\bar{\mathbf{u}}_i$  is the nodal displacement vector. The incremental strain–displacement relationships can be derived in a similar manner:

$$\Delta \boldsymbol{\varepsilon} = \sum_{i=1}^2 \mathbf{B}_i \Delta \bar{\mathbf{u}}_i \quad (23)$$

### Stress–Strain Relationships

The viscoelastic constitutive equation is solved by a finite difference method in the time domain consistent with refs. 3 and 13. In this method, at time  $t_{n+1}$ , the stresses are evaluated on the basis of the stress state at time  $t_n$ , plus the effect of the temperature and pressure history up to  $t_{n+1}$ . The

stress–strain relationships with incremental strains can be written as follows:

$$\boldsymbol{\sigma} = \mathbf{H} \Delta \boldsymbol{\varepsilon} + \mathbf{h} \quad (24)$$

where  $\boldsymbol{\sigma}$  is the stress tensor,  $\Delta \boldsymbol{\varepsilon}$  is the strain increment tensor,  $\mathbf{H}$  is the rigidity matrix to be determined by the viscoelastic relaxation data,

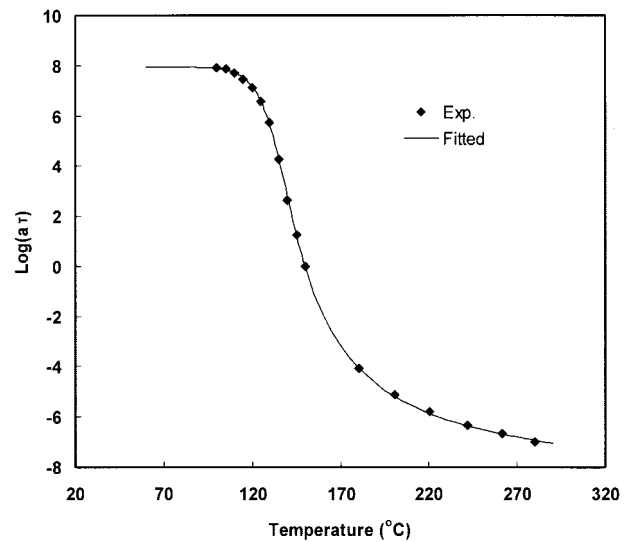


**Figure 7.** Time–temperature shift factor of PC (refer to the text for the fitted models).

and  $\mathbf{h}$  is a history vector. Detailed derivations of  $\mathbf{H}$  and  $\mathbf{h}$  can be found in ref. 13.

### Stiffness Matrices and Load Vectors

Derived from the principle of virtual work, the set of linear equations to be solved can be written as follows:

$$\mathbf{K}\Delta\mathbf{D} = \mathbf{R} \quad (25)$$

where  $\mathbf{K}$  is the global stiffness matrix,  $\Delta\mathbf{D}$  is the displacement increment vector to be solved, and  $\mathbf{R}$  is the right-hand side vector.

The element stiffness matrices can be written as follows:

$$\mathbf{k}^e = \int_V \mathbf{B}^T \mathbf{H} \mathbf{B} dV = 2\pi \int_{-d/2}^{d/2} \int_{r_1}^{r_2} \mathbf{B}^T \mathbf{H} \mathbf{B} r dr dz \quad (26)$$

where  $\mathbf{B}$  is the strain–displacement vector defined in eq 22,  $\mathbf{H}$  is the viscoelastic rigidity matrix defined in eq 24,  $d$  is the thickness of the disc, and  $r_1$  and  $r_2$  are the radii of the two nodes.

The element right-hand side vector can be written as follows:

$$\begin{aligned} \mathbf{R}^e &= \int_V (\mathbf{N}^T \mathbf{f} - \mathbf{B}^T \mathbf{h}) dV \\ &= 2\pi \int_{-d/2}^{d/2} \int_{r_1}^{r_2} (\mathbf{N}^T \mathbf{f} - \mathbf{B}^T \mathbf{h}) r dr dz \quad (27) \end{aligned}$$

where  $\mathbf{N}$  is the shape function vector,  $\mathbf{f}$  is the body force vector, and  $\mathbf{h}$  is the history vector defined in eq 24.

The numerical integration over the thickness is implemented by the trapezoidal rule, and the numerical integration over the radial direction is implemented by the Gauss quadrature for both element stiffness matrices and element right-hand side vectors.

### Boundary Conditions

For in-mold,

1.  $\sigma_{zz} = -P$ , where  $P$  is the pressure in the mold cavity.

**Table 7.** Screw Speed as a Function of Position

Position (mm)	31.50	29.00	25.00	6.00	3.50
Speed (mm/s)		80.0	100.0	120.0	80.0

2.  $\Delta\varepsilon_{rr} = \Delta\varepsilon_{\theta\theta} = 0$  and  $\Delta\varepsilon_{zz} \neq 0$ . The only nonzero strain increment is in the thickness direction.

Condition 2 is equivalent to a no-slip boundary condition on the mold walls. The radial and hoop strains are zero, with only displacement in the thickness direction allowed. This condition is especially true for injection–compression molding, in which the compression is in the  $z$  direction. In fact, any radial displacement would harm the microreplication of the data features on the discs. Because  $\Delta\varepsilon_{zz}$  can be obtained directly, there is no need to calculate the displacements by FEA. The stress components are directly calculated by  $\boldsymbol{\sigma} = \mathbf{h}$ .

For free quench,

1.  $\sigma_{zz} = 0$ , which is the plane-strain condition.
2.  $\Delta\varepsilon_{rr} \neq 0$ ,  $\Delta\varepsilon_{\theta\theta} \neq 0$ , and  $\Delta\varepsilon_{zz} \neq 0$ . All strains are nonzero, and the disc is free to deform.

The displacement field is solved by the finite element method. No boundary conditions should be applied during free quenching except for the displacement constraints to prevent rigid body movement.

## RESULTS AND DISCUSSION

CD-R substrates are injection–compression-molded according to the following processing conditions. The flow rate is controlled by the screw speed, which is profiled to be slow at the start of injection and to increase with the disc radius to best maintain a constant melt front velocity during the filling stage. A four-stage screw-speed profile is listed in Table 7. The diameter of the screw is 28 mm. A three-step clamp-force profile is used to allow the mold to open (breathe) during the filling to promote flow and then to close during the packing to promote pressure uniformity and feature replication. The profile is listed in Table 8. To study the effects of the melt temperature, mold coolant temperature, and packing pressure on warpage, we have performed a three-level design of experiments (DOE) with the low, median, and

**Table 8.** Clamp Force as a Function of Time

Clamp force (kN)	267	196	133
Duration (s)	0.8	1.50	1.00
Ramp time (s)	0.2	0.10	0.50

high levels listed in Tables 9 and 10. The packing pressures are the values applied at the nozzle. After the packing, the machine switches to a back-pressure of 1.21 MPa.

Warpage of the discs is deliberately introduced in the experiments by the coolant temperature of the moving side being set 2 °C lower than that of the stationary side, which is the nominal mold temperature. Because of the further temperature difference induced by the location of the gates and the stochastic deviation of the actual temperatures from the set points, the temperature difference is expanded to 5 °C in the simulation, and this temperature difference is used consistently for all DOE runs.

After ejection and further cooling, the discs were stacked in a spindle. The warpage of the molded CD-R substrates was then measured at every millimeter of the radius from  $r = 27$  mm to  $r = 57$  mm. Five discs from each DOE run were measured for minimum and maximum deflection at each radial location, and the 10 measurements were then averaged to obtain the mean value of the deflection. A zero vertical displacement constraint was applied in FEA at the stacking ring ( $r = 18$  mm), where the discs were in contact when stacked in a spindle, to prevent rigid body movement.

### Direction of Warpage

To investigate in what direction the discs tend to warp, we first perform a numerical simulation with no gravity effect. Figure 8 provides the simulation results for two DOE runs at low and high mold temperatures, with other processing conditions set to median values. In these and all figures plotting the vertical displacement, negative values correspond to the disc warpage toward the hot side. The simulation results show that at a low

**Table 9.** Melt and Mold Temperatures in DOE

Level	Low	Median	High
Melt temperature (°C)	300	310	320
Mold temperature (°C)	100	107	114

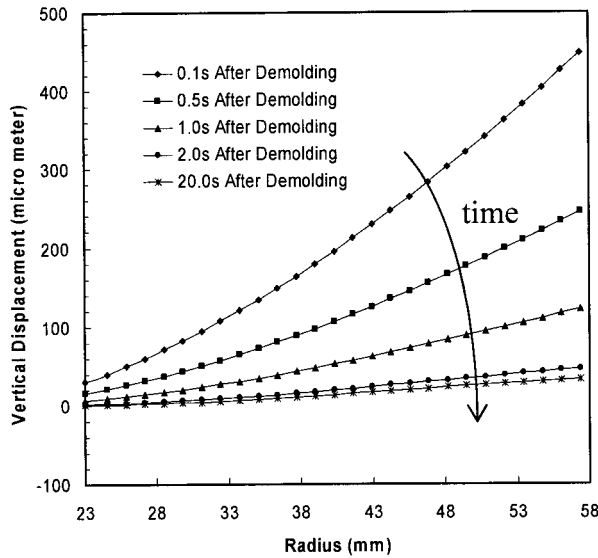
**Table 10.** Packing Pressure as a Function of Time in DOE

Time (s)	0.05	0.15	0.40
Low (MPa)	14.55	6.06	0.00
Median (MPa)	30.30	18.18	6.06
High (MPa)	48.48	24.24	12.12

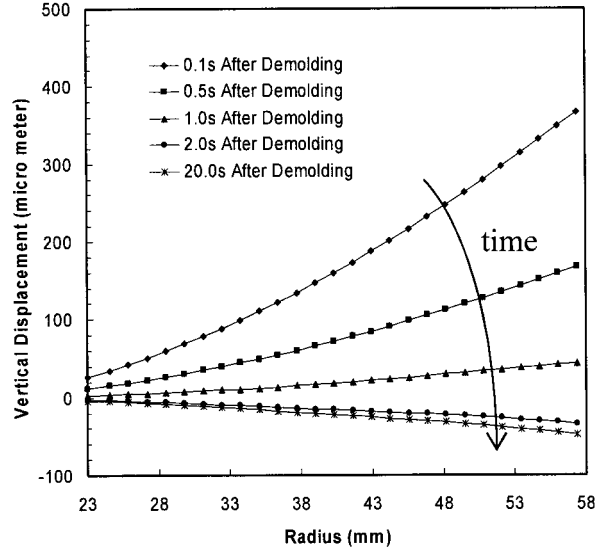
mold temperature (100 °C), the discs consistently warp to the cold side of the mold, whereas at a high mold temperature (114 °C), the discs warp consistently toward the hot side of the mold.

To understand this behavior, we provide the gapwise distributions of thermal stress for a DOE run with a low mold temperature just before demolding, just after demolding, and with 20 s of free quench in Figure 9. Other processing conditions are set to median values for this DOE run. Before the demolding, the stress is dominantly compressive because of the high cavity pressure during the filling and packing stages. The gapwise distribution of the thermal stress is not symmetrical with respect to the mid-plane because of the differential mold wall temperatures. The stress in the left, hot side of the disc is more compressive than that in the cold side because the temperature decay of the hot side is slower than that of the cold side. After the demolding, the disc is free to deform, and the asymmetric internal stress causes the warpage of the disc to develop. Because the temperature in the disc is still high and the disc is not stiff, the disc immediately warps toward the cold side upon ejection. As the disc further cools down in the air, tensile stresses develop in the core, and additional compressive stresses develop at the top and bottom surfaces of the disc. Because the hot side of the disc has a higher temperature than the cold side, it is less stiff and experiences more cooling than the cold side as the whole disc eventually cools down to room temperature. Therefore, the hot side will deform more than the cold side during the free quench of the disc, and this will cause the warpage to be less and less toward the cold side. At some point, the disc may pass the zero value and warp toward the hot side; that is, the disc warpage flips direction during cooling. Interestingly, the flipping of disc warpage was experimentally observed by other researchers.<sup>14</sup>

As shown in Figure 8, the discs warp to the cold side immediately after demolding at both low and high mold temperatures. The magnitude of the maximum vertical displacement at a low mold temperature is greater than that at a high mold temperature because of the different asymmetry of the



(a)



(b)

**Figure 8.** Simulated warpage development at (a) low and (b) high mold temperatures without the gravity effect.

stress and relaxation modulus. The hot side of the disc molded at a low mold temperature is stiffer and experiences less cooling during the free quench than the disc molded at a high mold temperature. The combined effect is that the final warpage at a low mold temperature is toward the cold side. For a high mold temperature, the warpage passes the zero value and continues to develop toward the hot

side, and this results in the final warpage toward the hot side. The eventual warpage direction toward the hot side or cold side depends on the mold temperature, the temperature difference, and the viscoelasticity of the material. Because the warpage is a result of the coupling between the temperature development of the disc and the relaxation modulus of the material, a fully viscoelastic model is required to accurately predict the warpage. Thermoelastic calculations ignoring the viscoelastic properties of polymers cannot predict the warpage development accurately.

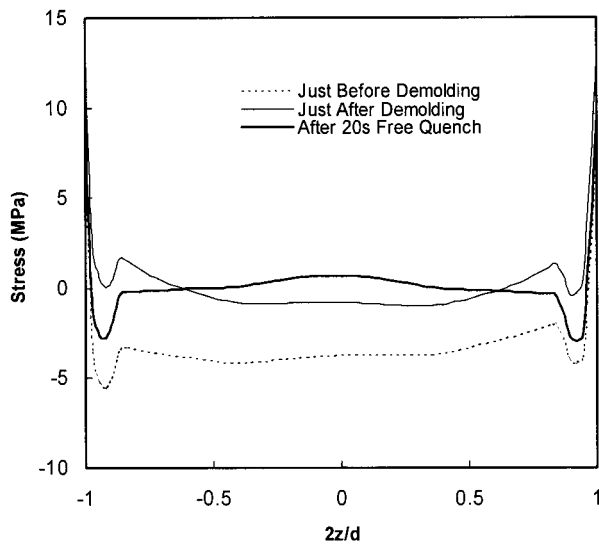


**Figure 9.** Thermal stress gapwise distributions at different times for low mold temperatures.

### Effect of Gravity

The vertical displacements of the molded discs as a function of the radius ( $r$ ) for two DOE runs with low (100 °C) and high (114 °C) mold temperatures are shown in Figure 10, with other processing conditions set to median values. The data points are the mean values of the measured vertical displacement, and the error bars are their 95% confidence intervals based on the 10 measurements. An inspection of the vertical displacement indicates that the predicted warpage (cf. final displacement of Fig. 8) varies significantly from the observed warpage of molded discs. Specifically, the curvature of the vertical displacement of the discs as a function of the radius also varies from

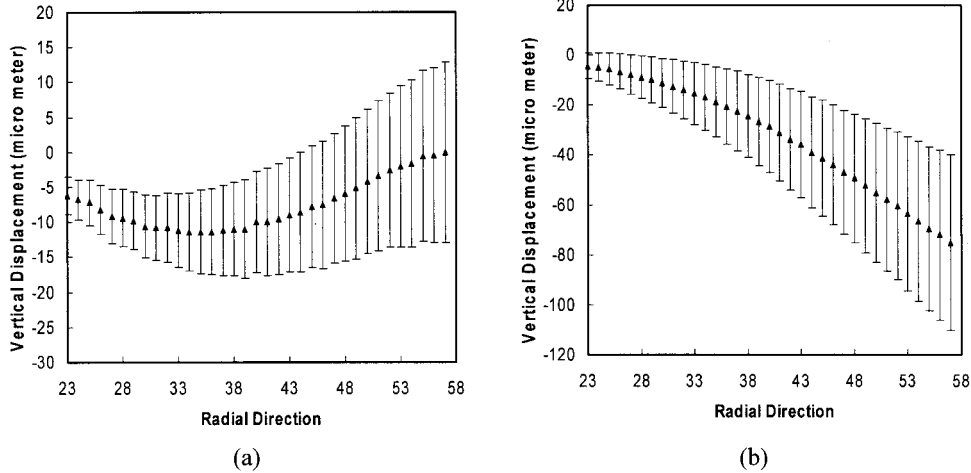


**Figure 10.** Measured warpage of discs at (a) low and (b) high mold temperatures. The error bars are the 95% confidence intervals for the measured warpage.

the initial simulation results. At lower mold temperatures, as shown in Figure 10(a), the disc warps to the hot side at radii of 28–35 mm and then back toward the cold side at the disc extremities. As the mold temperature increases to 114 °C, as shown in Figure 10(b), the disc monotonically warps to the hot side.

The observation of this warpage behavior has led to the supposition that gravity hinders the free development of the warpage and causes the complicated shape of the vertical deflection curve as a function of the disc radius. This theory is verified by Figure 11, which shows the measured warpage curve at a low mold temperature and corresponding simulated warpage curves with and without gravity effects. As Figure 11 demonstrates, the disc warps monotonically to the cold side without the gravity effect. With gravity, however, the disc warps to the hot side at radii of up to about 35 mm and then back toward the cold side at radii greater than 35 mm. Clearly, the results from the simulation including the gravity effect are closer to the experimental data.

**Effect of the Processing Conditions**

The simulated warpage and the experimental data under median processing conditions is shown in Figure 12, which is used as a benchmark for studying the effects of the processing conditions on the warpage. Warpage under different processing conditions is studied, and their main effects are compared with the experimental obser-

vations. All subsequent simulation results consider the gravity effects.

**Effect of the Melt Temperature**

To study the effects of the melt temperature on the warpage of the molded discs, we have used low and high melt temperatures, with other processing conditions set to the median values. The experimental and simulated vertical displacements for the two DOE runs with low and high melt temperatures are shown in Figure 13. As can

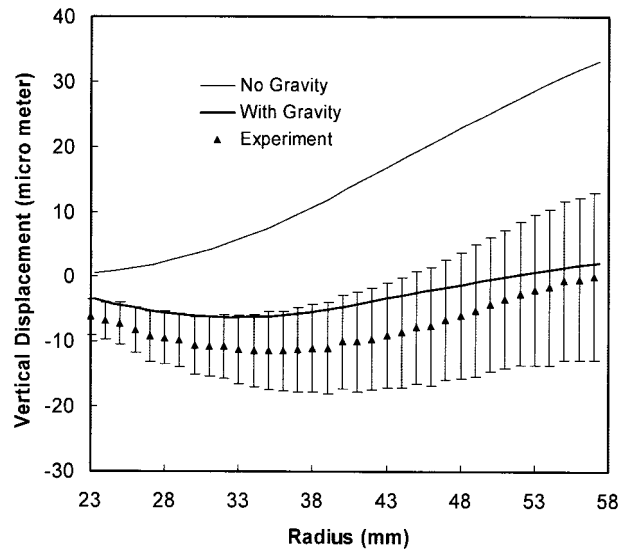


**Figure 11.** Comparison of the measured warpage and simulated warpage with and without the gravity effect.

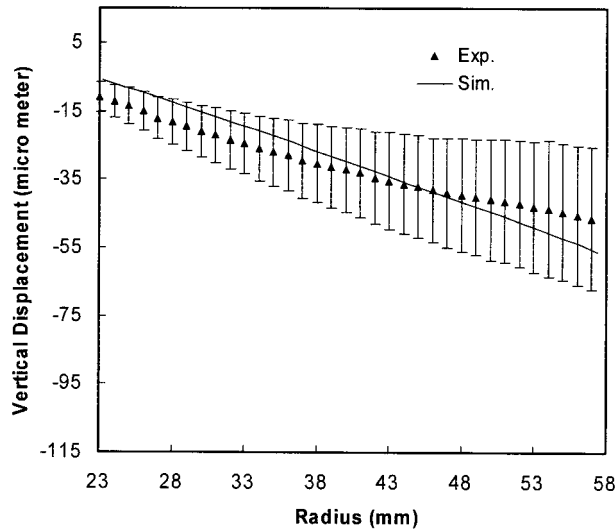


**Figure 12.** Warpage of a disc under the median processing condition. The error bars are the 95% confidence intervals for the measured warpage.

be observed in the figure, the simulation results agree with the mean values of the measured warpage data quantitatively. The main effect of the melt temperature on warpage is shown later in Figure 16(a). In the simulation, as the melt temperature increases from the low value to the median, the warpage slightly increases, but in the experiment, the warpage slightly decreases. As the melt temperature increases from the median value to the high value, the warpage increases both in the simulation and in the experiment. Nonetheless, the simulation values fall into the

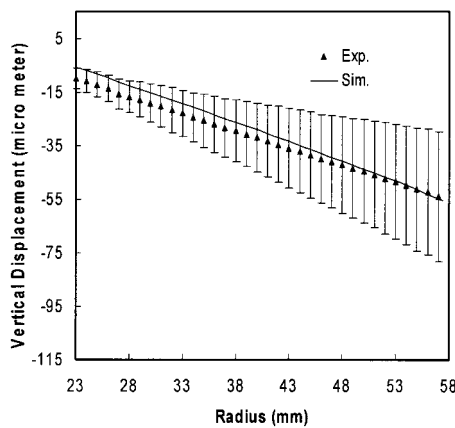
95% confidence intervals of the mean measured values of the vertical displacement.

**Effect of the Mold Temperature**

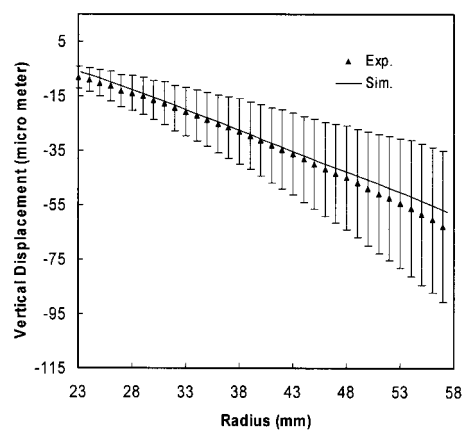
The experimental and simulated vertical displacements for the two DOE runs with low and high mold temperatures are shown in Figure 14. Other processing conditions are set to the median values. It can be seen from Figure 14 that the mold temperature has a great effect on warpage. With the mold temperature reduced from 114 to 100 °C, the maximum vertical displacement decreases from around 80 to around 10 μm. The main effect of the mold temperature on warpage is shown later in Figure 16(b). Both the simulation and experiment show that a higher mold temperature leads to a greater magnitude of warpage.

**Effect of the Packing Pressure**

The experimental and simulated vertical displacements for the two DOE runs with low and high packing pressures are shown in Figure 15. Other processing conditions are set to median values. For the DOE run with a low packing pressure, the simulated vertical displacement agrees qualitatively with the mean values of the warpage measurements, but the simulation underpredicts the magnitude of the warpage. For the DOE run with a high packing pressure, the simulation underpredicts the warpage value for lower radii but overpredicts the warpage value for higher radii, although the simulation results fall into the 95% confidence intervals of the mean values of



(a)



(b)

**Figure 13.** Warpage of discs at different melt temperatures: (a) 300 and (b) 320 °C. The error bars are the 95% confidence intervals of the measured warpage.

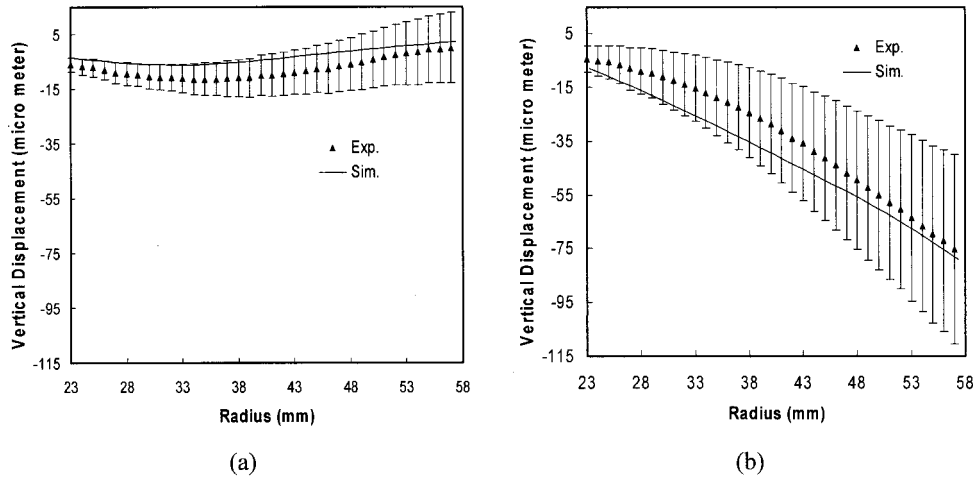


**Figure 14.** Warpage of discs at different mold temperatures: (a) 100 and (b) 114 °C. The error bars are the 95% confidence intervals of the measured warpage.

the measured vertical displacement. The error may be attributed to the deviation of the packing pressure effect in the process simulation from the experimental observations, as previously described.<sup>4</sup> The main effect of the packing pressure on the warpage is shown in Figure 16(c). Both the simulation and experiment show that the maximum vertical displacement increases as the packing pressure increases. This phenomenon is the opposite of that found in the experimental observations in ref. <sup>14</sup> for injection-molded discs, where it is observed that warpage decreases as packing

pressure increases. The reason might be the difference between the injection molding previously used and the injection-compression-molding processes used in this validation. It also should be noted that the packing time in this study is very short (0.4 s), and the postpacking cavity pressure is primarily determined by the clamp tonnage because of the compression.

**Summary**

Figure 16 provides the main effect plots comparing the simulated and experimental maximum

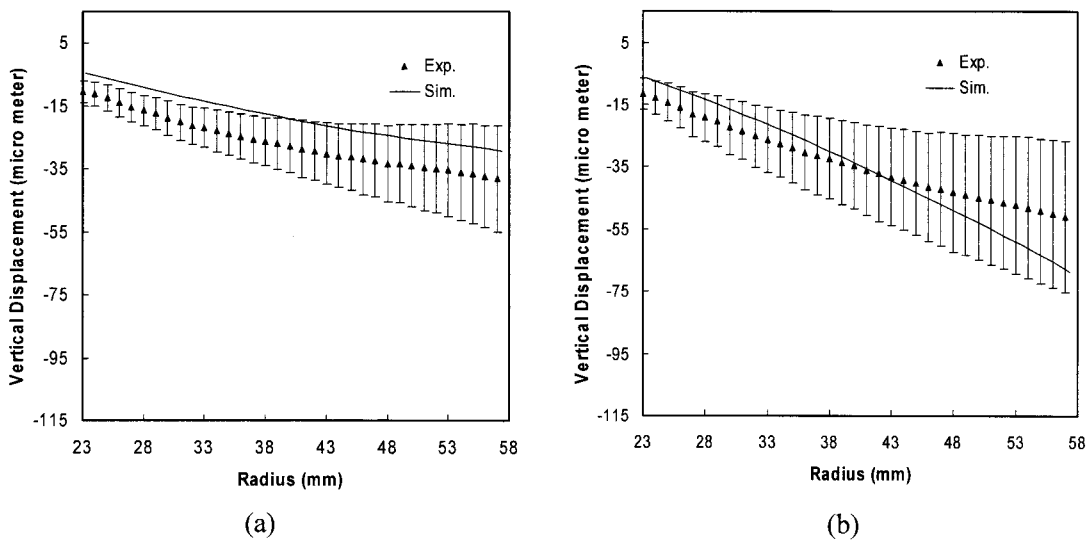


**Figure 15.** Warpage of discs under different packing pressures: (a) 2.45 MPa maximum and (b) 0.40 MPa maximum. The error bars are the 95% confidence intervals of the measured warpage.

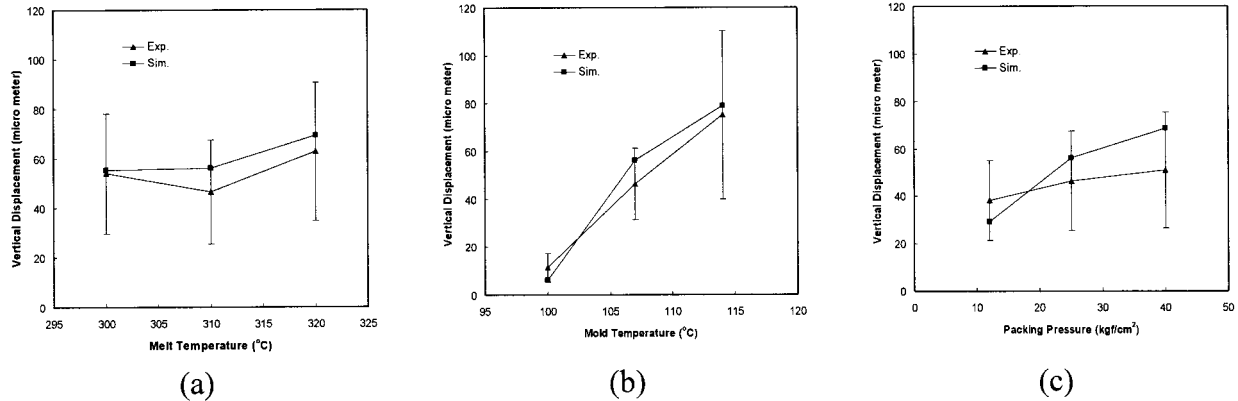


**Figure 16.** Summary of the main effect plots of warpage (absolute value): (a) melt temperature, (b) mold temperature, and (c) packing pressure. The error bars are the 95% confidence intervals of the measured warpage.

vertical displacement. As can be seen, the simulation well predicts the effects of various processing conditions, and the correlations between the simulation and the experiment are very close. Therefore, the simulation provides vital insights into the various causes of warpage and can provide valuable assistance in material and process development to reduce the warpage of optical media during mass production.

## CONCLUSIONS

A numerical simulation of thermally induced stress and warpage of injection-compression-molded discs with a viscoelastic material model has been developed. A finite element formulation has been employed with axisymmetric plate elements to simulate the warpage of the injection-compression-molded discs after demolding. Simulation results of CD-R moldings under different processing conditions, such as the melt temperature, mold temperature, and packing pressure, have been compared with experimental observations. A good agreement of simulation results and experimental data has been observed. The simulation shows that gravity has a significant effect on the magnitude and curvature behavior of disc warpage, and to accurately predict the development of warpage over time, we need a viscoelastic constitutive model.

The authors acknowledge Sam Miller (GE Plastics) and Irene Dris (GE Corporate Research and Development)

for providing the material data and colleagues in the Optical Media Development Center of GE Plastics for enabling validation of the warpage simulation.

## REFERENCES AND NOTES

1. Paro, H. T.; Bosnyak, C. P.; Sehanobish, K. *Machine Des* 1986, 58, 69.
2. Isayav, A. I.; Crouthamel, D. L. *Polym Plast Tech Eng* 1984, 22, 177.
3. Baaijens, F. P. T. *Rheol Acta* 1991, 30, 284.
4. Fan, B.; Kazmer, D.; Theriault, R.; Poslinski, A. *Polym Eng Sci*, in press.
5. Krevelen, D. W. V. *Properties of Polymers*; Elsevier: Amsterdam, 1976.
6. Cross, M. M. *Rheol Acta* 1979, 18, 609.
7. Chiang, H. H.; Hieber, C. A.; Wang, K. K. *Polym Eng Sci* 1991, 31, 116.
8. Ferry, J. D. *Viscoelastic Properties of Polymers*; Wiley: New York, 1980.
9. Rockey, K. C.; Evans, H. R.; Griffiths, D. W. *The Finite Element Method*; Wiley: New York, 1983.
10. Zienkiewicz, O. C. *The Finite Element Method in Engineering and Science*; McGraw-Hill: London, 1971.
11. Hughes, T. J. R. *The Finite Element Method*; Dover: New York, 2000.
12. Hinton, E.; Owen, D. R. J. *Finite Element Software for Plates and Shells*; Pineridge: Swansea, U.K., 1984.
13. Douven, L. F. A. Ph.D. Thesis, Eindhoven University of Technology, 1991.
14. Denizart, O.; Vincent, M.; Agassant, J. F. *J Mater Sci* 1995, 30, 552.